Int. J. Heat Mass Transfer. Vol. 23, pp. 451–461.

0017–9310/80/0401–0451 $02.00/0

COMBINED HEAT AND MASS TRANSFER IN NATURAL CONVECTION ALONG A VERTICAL CYLINDER

T. S. CHEN and C. F. YUH

Department of Mechanical and Aerospace Engineering, University of Missouri-Rolla, Rolla, MO 65401, U.S.A.

(*Received* 29 *May* 1979 *and in revised form* 4 *September* 1979)

Abstracts – An analytical study is performed to examine the heat- and mass-transfer characteristics of natural convection flow along a vertical cylinder under the combined buoyancy force effects of thermal and species diffusion. The analysis is restricted to processes in which the diffusion-thermo and thermo-diffusion effects as well as the interfacial velocities arising from species diffusion are negligible. The surface of the cylinder is either maintained at a uniform temperature/concentration or subjected to a uniform heat/mass flux. Among the major parameters of the problem are curvature of cylinder, Prandtl and Schmidt numbers, thermal and concentration Grashof numbers, and the relative buoyancy force effect between species and thermal diffusion. Numerical results are obtained and presented for species diffusion of interest in air and water. For both heating/diffusing conditions, the local wall shear stress, the local Nusselt number, and the local Sherwood number increase with increasing curvature of the cylinder. In addition, the first two quantities are found to increase and decrease as the buoyancy force from species diffusion assists and opposes, respectively, the thermal buoyancy force. The mass-transfer parameter or the local Sherwood number is enhanced as the thermal buoyancy force increases. Finally, the combined buoyancy force from thermal and species diffusion provides larger Nusselt and Sherwood numbers for uniform surface heat/mass flux than for uniform wall temperature/concentration.

NOMENCLATURE

C, species mass fraction or concentration;
D, binary diffusion coefficient;
f, F, reduced stream functions;
g, gravitational acceleration;
$Gr_{x,t}$, thermal Grashof number $g\beta(T_w - T_\infty)x^3/\nu^2$;
$Gr^*_{x,t}$, modified thermal Grashof number, $g\beta q_w x^4/k\nu^2$;
$Gr_{x,c}$, Grashof number for mass diffusion, $g\beta^*(C_w - C_\infty)x^3/\nu^2$;
$Gr^*_{x,c}$, modified Grashof number for mass diffusion, $g\beta^*\dot{m}_w x^4/\rho D\nu^2$;
k, thermal conductivity of the fluid;
$\dot{m}$, mass flux of the diffusing species;
N, ratio of Grashof numbers, $Gr_{x,c}/Gr_{x,t}$;
N^*, ratio of modified Grashof numbers, $Gr^*_{x,c}/Gr^*_{x,t}$;
Nu_x, local Nusselt number, $q_w x/[(T_w - T_\infty)k]$;
Pr, Prandtl number, ν/α;
q_w, local surface heat-transfer rate per unit area;
r_0, radius of cylinder;
Sc, Schmidt number, ν/D;
Sh_x, local Sherwood number, $\dot{m}_w x/[\rho D(C_w - C_\infty)]$;
T, fluid temperature;
u, v, velocity components in x and r directions;
x, r, axial and radial coordinates;
Y, modified pseudo-similarity variable;
Y_δ, modified dimensionless boundary-layer thickness.

Greek symbols

α, thermal diffusivity of the fluid;
β, volumetric coefficient of thermal expansion, $[-(\partial\rho/\partial T)_{p,C}]/\rho$;
β^*, volumetric coefficient of expansion with mass fraction, $[-(\partial\rho/\partial C)_{p,T}]/\rho$;
η, pseudo-similarity variable;
η_δ, dimensionless boundary-layer thickness;
θ, dimensionless temperature;
λ, dimensionless mass fraction;
μ, dynamic viscosity of the fluid;
ν, kinematic viscosity of the fluid;
ξ, dimensionless axial coordinate;
ρ, density of the fluid;
τ, shear stress;
ϕ, modified dimensionless temperature;
χ, modified dimensionless axial coordinate;
ψ, stream function;
ω, modified dimensionless mass fraction.

Subscripts

w, condition at the wall;
∞, condition at the free stream.

INTRODUCTION

MANY transport processes exist in nature and in industrial applications in which the transfer of heat and mass occurs simultaneously as a result of combined buoyancy effects of thermal diffusion and

diffusion of chemical species. The effects of mass diffusion on natural thermal convection flow have been widely investigated for vertical and horizontal flat plates. A summary of the past studies can be found, for example, in [1]. More studies have been reported for vertical and horizontal plates [1,2] and very recently for inclined plates [3]. These latter analyses were based on species diffusion processes with very low concentration level such that the diffusion-thermo effect and the thermo-diffusion effect, as well as the interfacial velocity at the wall due to species diffusion, were neglected. Solutions were obtained in a similarity form and numerical results were presented for a range of Schmidt numbers of common interest in air and water.

In contrast to vertical, inclined, and horizontal plates, the analysis of natural convection on a vertical cylinder has been confined to flow induced solely by the temperature variations (see, for instance, [4] and the studies cited therein). No analytical work on natural convection along a vertical cylinder under the combined effects of thermal and mass diffusion seems to have been reported. The main reason for a lack of analytical study on this problem can be attributed to the rather difficult mathematical and numerical procedures involved in dealing with the nonsimilar boundary layers. In view of the importance of simultaneous transfer of heat and mass in engineering applications, such a study for vertical cylinders is warranted. This has motivated the present investigation. In the analysis, consideration is given to situations in which the surface of the cylinder is either maintained at a uniform temperature and concentration or subjected to a uniform heat and mass flux. The conservation equations of the laminar boundary layer are first transformed into a nondimensional form and their solutions are then obtained by an efficient finite-difference method. Numerical results are presented for air (Pr = 0.7) over a Schmidt number range of Sc = 0.2–1.0 and for water (Pr = 7) over Sc = 7–500. They cover a range of diffusion species in air and water.

ANALYSIS

Consider a vertical cylinder of radius r_0 which is situated in an otherwise quiescent environment having temperature T_∞ and concentration C_∞. The surface of the cylinder is maintained at a uniform temperature T_w and uniform concentration C_w or is subjected to a uniform heat flux q_w and uniform mass flux $\dot{m}_w$. The axial and radial coordinates are taken to be x and r, with x measuring the distance along the centerline of the cylinder from its bottom end and r measuring normal to the axis of the cylinder. The gravitational force then acts in the opposite direction of x. The buoyancy force resulting from the concentration differences may assist or oppose the buoyancy force induced by the temperature variations in the fluid.

The analysis will be confined to species diffusion processes in which the diffusion-thermo and thermo-diffusion effects can be neglected. By employing the Boussinesq approximation, along with the conventional boundary-layer assumptions, the conservation equations of the laminar boundary layer can be written as

$$\frac{\partial}{\partial x}(ru) + \frac{\partial}{\partial r}(rv) = 0 \tag{1}$$

$$u\frac{\partial u}{\partial x} + v\frac{\partial u}{\partial r} = \nu\frac{1}{r}\frac{\partial}{\partial r}\left(r\frac{\partial u}{\partial r}\right) + g\beta(T - T_\infty) + g\beta^*(C - C_\infty) \tag{2}$$

$$u\frac{\partial T}{\partial x} + v\frac{\partial T}{\partial r} = \alpha\frac{1}{r}\frac{\partial}{\partial r}\left(r\frac{\partial T}{\partial r}\right) \tag{3}$$

$$u\frac{\partial C}{\partial x} + v\frac{\partial C}{\partial r} = D\frac{1}{r}\frac{\partial}{\partial r}\left(r\frac{\partial C}{\partial r}\right) \tag{4}$$

where the conventional notations are defined in the Nomenclature. Equations (1)–(4) are subject to the following boundary conditions

$$u = 0, \quad v = v_w \text{ at } r = r_0$$
$$T = T_w \text{ and } C = C_w \text{ or } q_w = -k\partial T/\partial r \text{ and } \dot{m}_w = -\rho D\partial C/\partial r \text{ at } r = r_0 \tag{5}$$
$$u \to 0, \quad T \to T_\infty, \quad C \to C_\infty \text{ as } r \to \infty$$
$$u = 0, \quad T = T_\infty, \quad C = C_\infty \text{ at } x = 0, \quad r \geq r_0.$$

The interfacial velocity v_w at the surface of the cylinder as a result of mass diffusion process will be neglected in the analysis. This is because consideration will be given to situations in which the concentration level is low. The validity and the condition for the neglect of v_w will be further discussed later.

Equations (1)–(5) do not admit a similarity solution. The nonsimilarity arises from the surface curvature of the cylinder. As the first step in the analysis, these equations are transformed into a dimensionless form. This will be done separately for the uniform wall temperature/concentration case and the uniform surface heat/mass flux case.

Uniform Wall Temperature/Concentration (UWT/UWC) case

For this case, one introduces the dimensionless axial coordinate $\xi(x)$ and the pseudosimilarity variable η

$$\xi = 2\frac{x}{r_0}(Gr_{x,t}/4)^{-1/4},$$
$$\eta = \frac{r^2 - r_0^2}{2r_0x}(Gr_{x,t}/4)^{1/4} \tag{6}$$

along with the dimensionless stream function $f(\xi,\eta)$, the dimensionless temperature $\theta(\xi,\eta)$, and the dimensionless concentration $\lambda(\xi,\eta)$ defined, respectively, by

$$f(\xi,\eta) = \psi(x,r)/[4\nu r_0(Gr_{x,t}/4)^{1/4}] \tag{7}$$
$$\theta(\xi,\eta) = (T - T_\infty)/(T_w - T_\infty),$$
$$\lambda(\xi,\eta) = (C - C_\infty)/(C_w - C_\infty) \tag{8}$$

where the stream function $\psi(x,r)$ satisfies the continuity equation (1) with

$$ru = \partial\psi/\partial r, \quad rv = -\partial\psi/\partial x. \tag{9}$$

By introducing equations (6)–(9) into equations (2)–(5) one can arrive at the following system of equations:

$$(1+\xi\eta)f''' + (\xi+3f)f'' - 2f'^2 + \theta + N\lambda = \xi(f'\partial f'/\partial\xi - f''\partial f/\partial\xi) \tag{10}$$

$$\frac{1}{Pr}(1+\xi\eta)\theta'' + \left(\frac{\xi}{Pr}+3f\right)\theta' = \xi(f'\partial\theta/\partial\xi - \theta'\partial f/\partial\xi) \tag{11}$$

$$\frac{1}{Sc}(1+\xi\eta)\lambda'' + \left(\frac{\xi}{Sc}+3f\right)\lambda' = \xi(f'\partial\lambda/\partial\xi - \lambda'\partial f/\partial\xi) \tag{12}$$

$$f'(\xi,0) = 0, \quad 3f(\xi,0) + \xi\partial f(\xi,0)/\partial\xi = 0,$$
$$\theta(\xi,0) = \lambda(\xi,0) = 1, \tag{13}$$
$$f'(\xi,\infty) = \theta(\xi,\infty) = \lambda(\xi,\infty) = 0.$$

In the foregoing equations, the primes stand for partial derivatives with respect to η, Pr is the Prandtl number, Sc is the Schmidt number, and the quantity N has the expression

$$N = \frac{\beta^*(C_w - C_\infty)}{\beta(T_w - T_\infty)} = \frac{Gr_{x,c}}{Gr_{x,t}} \tag{14}$$

where the local thermal Grashof number $Gr_{x,t}$ and the local Grashof number for mass diffusion $Gr_{x,c}$ are given by

$$Gr_{x,t} = g\beta(T_w - T_\infty)x^3/\nu^2, \quad Gr_{x,c} = g\beta^*(C_w - C_\infty)x^3/\nu^2. \tag{15}$$

Thus, N represents the relative effect of chemical species diffusion on thermal diffusion. When $N = 0$, there is no mass diffusion and the buoyancy force arises solely from the temperature differences. The buoyancy forces from mass and thermal diffusion are combined to assist the flow when $N > 0$, whereas they oppose each other when $N < 0$.

In writing the boundary condition $3f(\xi,0) + \xi\partial f(\xi,0)/\partial\xi = 0$ in equation (13), the interfacial velocity at the surface, v_w, associated with the species diffusion has been neglected. This approximation can be justified if the condition

$$\frac{v_w x}{\nu} \ll (Gr_{x,t}/4)^{1/4} \tag{16}$$

or, with the use of Fick's law,

$$\frac{1}{Sc}(C_w - C_\infty)[-\lambda'(\xi,0)] \ll 1 \tag{17}$$

is fulfilled.

It must be pointed out that the $\xi(x)$ parameter appearing in equation (6) can be written as $\xi = (r^2 - r_0^2)/\eta r_0^2$ which is seen as a measure of the ratio of the boundary-layer thickness to the cylinder radius r_0. As a result, small values of ξ correspond to relatively thin boundary layers (compared to r_0) and hence to small deviations from a flat plate. On the other hand, large values of ξ correspond to relatively thick boundary layers and to large deviations from a flat plate. When $\xi = 0$, the problem reduces to a vertical flat plate. In addition, for very thin boundary layers, r does not differ appreciably from r_0 so that $(r^2 - r_0^2)/2r_0$ reduces to $r - r_0 = y$ and, as a consequence, the η variable reduces to the similarity variable for a flat plate.

The major physical quantities of interest are the local wall shear stress τ_w, the local Nusselt number Nu_x, and the local Sherwood number Sh_x. They are defined, respectively, by

$$\tau_w = \mu\left(\frac{\partial u}{\partial r}\right)_{r=r_0}, \quad Nu_x = \frac{q_w}{T_w - T_\infty}\frac{x}{k}, \quad Sh_x = \frac{\dot{m}_w}{(C_w - C_\infty)}\frac{x}{\rho D}. \tag{18}$$

By employing Fourier's law $q_w = -k(\partial T/\partial r)_{r=r_0}$ and Fick's law $\dot{m}_w = -\rho D(\partial C/\partial r)_{r=r_0}$, along with the expression for $(\partial u/\partial r)_{r=r_0}$, one can show that

$$\tau_w = 4\mu\nu x^{-2}(Gr_{x,t}/4)^{3/4}f''(\xi,0) \tag{19}$$

$$Nu_x(Gr_{x,t}/4)^{-1/4} = -\theta'(\xi,0) \tag{20}$$

$$Sh_x(Gr_{x,t}/4)^{-1/4} = Sh_x(|Gr_{x,c}/N|/4)^{-1/4} = -\lambda'(\xi,0). \tag{21}$$

Uniform Surface Heat/Mass Flux (UHF/UMF) case

The dimensionless coordinates for this case are given by

$$\chi = 2\frac{x}{r_0}(Gr^*_{x,t}/5)^{-1/5}, \quad Y = \frac{r^2 - r_0^2}{2r_0 x}(Gr^*_{x,t}/5)^{1/5} \tag{22}$$

and the dimensionless stream function $F(\chi, Y)$, temperature $\phi(\chi, Y)$, and concentration $\omega(\chi, Y)$ by

$$F(\chi,Y) = \psi(x,r)/[5\nu r_0(Gr^*_{x,t}/5)^{1/5}] \tag{23}$$

$$\phi(\chi,Y) = (T - T_\infty)(Gr^*_{x,t}/5)^{1/5}/(q_w x/k) \tag{24}$$

$$\omega(\chi,Y) = (C - C_\infty)(Gr^*_{x,t}/5)^{1/5}/(\dot{m}_w x/\rho D). \tag{25}$$

Introduction of equations (22)–(25) and (9) into equations (1)–(5) leads to the system of equations

$$(1+\chi Y)F''' + (\chi+4F)F'' - 3F'^2 + \phi + N^*\omega = \chi(F'\partial F'/\partial\chi - F''\partial F/\partial\chi) \tag{26}$$

$$\frac{1}{Pr}(1+\chi Y)\phi'' + \left(\frac{\chi}{Pr}+4F\right)\phi' - F'\phi = \chi(F'\partial\phi/\partial\chi - \phi'\partial F/\partial\chi) \tag{27}$$

$$\frac{1}{Sc}(1+\chi Y)\omega'' + \left(\frac{\chi}{Sc}+4F\right)\omega' - F'\omega = \chi(F'\partial\omega/\partial\chi - \omega'\partial F/\partial\chi) \tag{28}$$

$$F'(\chi,0)=0,\quad 4F(\chi,0)+\chi\,\partial F(\chi,0)/\partial\chi=0$$
$$\phi'(\chi,0)=\omega'(\chi,0)=-1, \tag{29}$$
$$F'(\chi,\infty)=\phi(\chi,\infty)=\omega(\chi,\infty)=0.$$

The quantity N^* in equation (26) measures the relative effect of mass and thermal diffusion and is given by

$$N^*=(\beta^*\dot{m}_w/\rho D)/(\beta q_w/k)=Gr^*_{x,c}/Gr^*_{x,t} \tag{30}$$

where

$$Gr^*_{x,c}=g\beta^*\dot{m}_w x^4/\rho D\nu^2,\quad Gr^*_{x,t}=g\beta q_w x^4/k\nu^2 \tag{31}$$

are, respectively, the modified Grashof numbers for mass and thermal diffusion. The buoyancy effects of mass and thermal diffusion are combined to assist the flow when $N^*>0$ and to oppose the flow when $N^*<0$. There is no buoyancy force from mass diffusion when $N^*=0$.

The boundary condition $4F(\chi,0)+\chi\,\partial F(\chi,0)/\partial\chi=0$ in equation (18), which is obtained by neglecting the interfacial velocity v_w at the surface due to the mass diffusion, is valid when the condition

$$\frac{v_w x}{\nu}\ll(Gr^*_{x,t}/5)^{1/5} \tag{32}$$

or equivalently the condition

$$\frac{1}{Sc}\frac{(C_w-C_\infty)}{\omega(\chi,0)}\ll 1 \tag{33}$$

is fulfilled.

The wall shear stress, the local Nusselt number, and the local Sherwood number as defined by equation (18) now lead, respectively, to the expressions

$$\tau_w=5\,\mu\nu x^{-2}(Gr^*_{x,t}/5)^{3/5}F''(\chi,0) \tag{34}$$
$$Nu_x(Gr^*_{x,t}/5)^{-1/5}=1/\phi(\chi,0) \tag{35}$$
$$Sh_x(Gr^*_{x,t}/5)^{-1/5}=Sh_x(|Gr^*_{x,c}/5N^*|)^{-1/5}=1/\omega(\chi,0). \tag{36}$$

Comparisons between UWT/UWC and UHF/UMF cases

It is interesting to compare the results between the uniform wall temperature/concentration (UWT/UWC) case and the uniform surface heat/mass flux (UHF/UMF) case. This comparison will be done for the local Nusselt numbers and the local Sherwood numbers. To facilitate such a comparison, it is necessary to define an equivalent axial coordinate for thermal diffusion ξ_e for the UHF case in terms of the local wall temperature $T_w(x)$ and an equivalent axial coordinate for mass diffusion $\xi_{c,e}$ for the UMF case in terms of the local wall concentration $C_w(x)$. Let

$$\xi_e=\frac{2x}{r_0}[|(Gr_{x,t})_e|/4]^{-1/4} \tag{37}$$

$$\xi_{c,e}=\frac{2x}{r_0}[|(Gr_{x,c})_e|/4]^{-1/4} \tag{38}$$

where

$$(Gr_{x,t})_e=\frac{g\beta[T_w(x)-T_\infty]x^3}{\nu^2},$$
$$(Gr_{x,c})_e=\frac{g\beta^*[C_w(x)-C_\infty]x^3}{\nu^2} \tag{39}$$

and

$$T_w(x)-T_\infty=(q_w x/k)(Gr^*_{x,t}/5)^{1/5}\phi(\chi,0) \tag{40}$$
$$C_w(x)-C_\infty=(\dot{m}_w x/\rho D)(Gr^*_{x,t}/5)^{1/5}\omega(\chi,0) \tag{41}$$

from equations (24) and (25), respectively.

Substituting equation (40) into equation (37) one obtains, with the aid of χ definition in equation (22), that

$$\xi_e=\chi[(5/4)\phi(\chi,0)]^{-1/4}. \tag{42}$$

Similarly, by substituting equation (41) into equation (38), one arrives at

$$\xi_{c,e}=\chi[(5/4)N^*\omega(\chi,0)]^{-1/4}. \tag{43}$$

Thus, for $\xi=\xi_e$ as given by equation (42), one finds from equations (20) and (35) that

$$\frac{(Nu_x)_{UHF}}{(Nu_x)_{UWT}}=\frac{(4/5)^{1/4}}{[-\theta'(\xi,0)][\phi(\chi,0)]^{5/4}}. \tag{44}$$

Similarly, for $\xi_c=\xi_{c,e}$, one can find the Sherwood number ratio as

$$\frac{(Sh_x)_{UMF}}{(Sh_x)_{UWC}}=\frac{(4/5)^{1/4}}{[-\lambda'(\xi,0)][\phi(\chi,0)]^{1/4}[\omega(\chi,0)]}. \tag{45}$$

To determine the local Nusselt number and the local Sherwood number ratios, the relationship between N^* and N needs to be known. From the definition of N and N^* it can be shown that

$$N^*/N=\phi(\chi,0)/\omega(\chi,0) \tag{46}$$

when $\xi=\xi_e$. With this, a comparison between equation (42) and equation (43) yields the relationship

$$\xi_{c,e}=\xi_e/N^{1/4}. \tag{47}$$

In the situation in which $Sc=Pr$, the ϕ and ω functions, equations (27) and (28), become identical and $\phi(\chi,0)=\omega(\chi,0)$. This leads to $N^*=N$ from equation (46) when $\xi=\xi_e$. In addition, equations (11) and (12) give $\theta'(\xi,0)=\lambda'(\xi,0)$ when $Sc=Pr$. This then leads to $N^*=N$ when $\xi=\xi_e$. Thus, under the conditions $Sc=Pr$, $\xi=\xi_e$, and $N^*=N$, the local Sherwood number ratio and the local Nusselt number ratio as given, respectively, by equations (45) and (44) become exactly identical. The numerical results for these ratios will be presented later.

NUMERICAL SOLUTIONS

The two systems of partial differential equations, equations (10)–(13) and (26)–(29), are coupled, respectively, through the functions f, θ, λ and F, ϕ, ω for parametric values of N, Pr, Sc for the former and N^*, Pr, Sc for the latter. In the present study, these

equations were solved by an accurate finite-difference method. This method is a modified version of the method described in [5] for solutions of uncoupled equations. To begin with, the partial differential equations (10)–(12) or (26)–(28) are first converted into a system of first order equations which are then expressed in finite-difference form by approximating the functions and their first derivatives in terms of centered difference and averages at midpoints of the net segments in the (ξ, η) or (χ, Y) coordinates or the net rectangles in the (ξ, η) or (χ, Y) domains. The resulting nonlinear finite difference equations are then solved by Newton's iterative method.

In the computations for the uniform wall temperature/concentration (UWT/UWC) case, the ξ values were varied from 0 to about 10 and the values of the parameter N from -0.5 to 1.0, with Schmidt numbers ranging from 0.2 to 1.0 for $Pr = 0.7$ and from 7 to 500 for $Pr = 7$. For the case of uniform surface heat/mass flux, the χ values were varied from 0 to 5 and the N^* values from -0.5 to 1.0, with Schmidt numbers of 0.6 to 1.0 for $Pr = 0.7$ and 7 to 500 for $Pr = 7$. While a step size of $\Delta\xi$ or $\Delta\chi$ of 0.25 was found to be sufficient for the entire ξ or χ range investigated, the step sizes for $\Delta\eta$ or ΔY were varied from the standpoints of accuracy and economy. For the UWT/UWC case with $Pr = 0.7$, $\Delta\eta$ was increased step by step from 0.02 for $0 \leq \eta \leq 6$, 0.04 for $6 \leq \eta \leq 15$, 0.08 for $15 \leq \eta \leq 30$, 0.25 for $30 \leq \eta \leq 80$, 2.0 for $80 \leq \eta \leq 350$, to 5.0 for $\eta > 350$. The η_δ values were varied from 10 to about 500 as ξ increased from 0 to about 10. Similar increases in step sizes were employed for the UHF/UMF case over the Y_δ range of 10 to 200 as χ varied from 0. to 5. However, for very high Schmidt numbers, such as $Sc = 100$ and 500, that are associated with $Pr = 7$, the mass fraction boundary layer becomes very thin ($\eta < 1$) as compared to the flow and thermal boundary layers, and smaller step sizes of $\Delta\eta = 0.005$ for $0 \leq \eta \leq 1$ and $\Delta Y = 0.002$ for $0 \leq Y \leq 1$ were additionally used, respectively, for the UWT/UWC and UHF/UMF cases to provide accurate results. The Schmidt number range for $Pr = 0.7$ covers diffusion into air of hydrogen ($Sc = 0.22$), water vapor (0.6), carbon dioxide (0.94) and methanol (0.97). For $Pr = 7$, a Schmidt number of 500 covers closely the diffusion into water of ammonia ($Sc = 445$), carbon dioxide (453), sulfur dioxide (523), methanol (556), sodium chloride (580), and chlorine (617).

RESULTS AND DISCUSSION

Figures 1–3 illustrate, respectively, the local wall shear stress, the local Nusselt number, and the local Sherwood number as a function of ξ for the UWT/UWC case, covering various parametric values of N and Sc for $Pr = 0.7$ and 7. Similar plots for the UHF/UMF case are shown, respectively, in Figs. 4–6 as a function of χ. It is noted that both ξ and χ are not only a measure of the curvature of the cylinder, but also a measure of the ratio of the boundary-layer thickness to the cylinder radius r_0, because they can be represented, respectively, as $\xi = (r^2 - r_0^2)/r_0^2\eta$ and $\chi = (r^2 - r_0^2)/r_0^2 Y$. Thus, small values of ξ or χ represent thin boundary layers compared to r_0 and hence small deviations from a flat plate, with $\xi = 0$ or $\chi = 0$ corresponding exactly to a vertical flat plate. On the other hand, large values of ξ or χ correspond to relatively thick boundary layers and hence to large departures from a flat plate. It should be noted, however, that $\xi = 0$ or $\chi = 0$ implies that $r_0 \to \infty$.

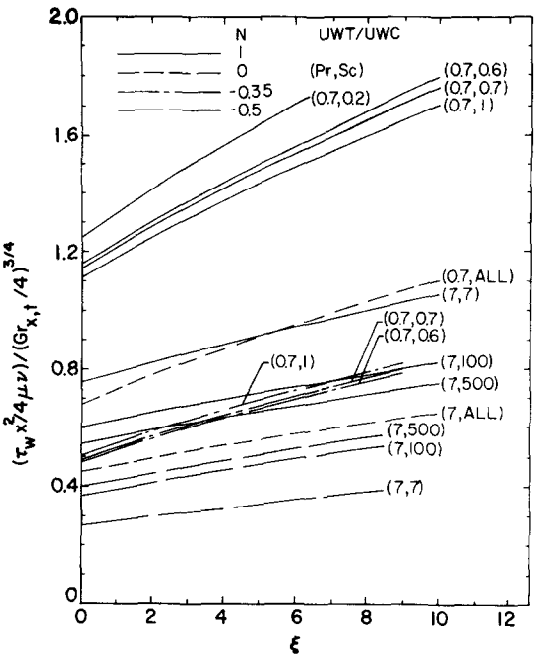

FIG. 1. Local wall shear results for uniform wall temperature/concentration, $Pr = 0.7$ and 7.

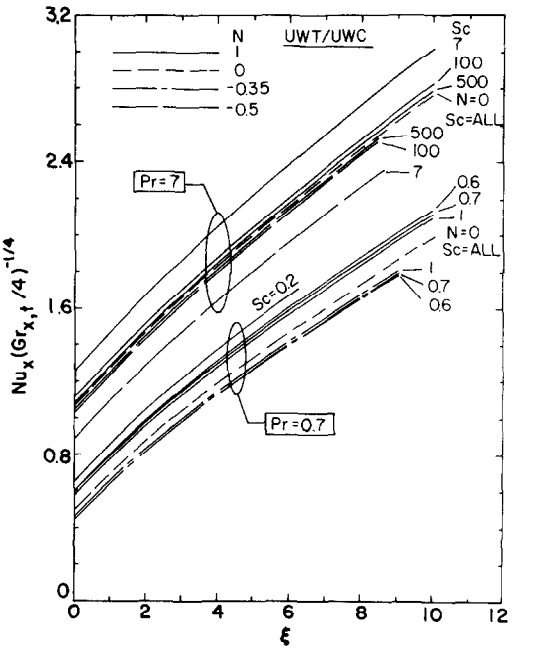

FIG. 2. Local Nusselt number results for uniform wall temperature/concentration, $Pr = 0.7$ and 7.

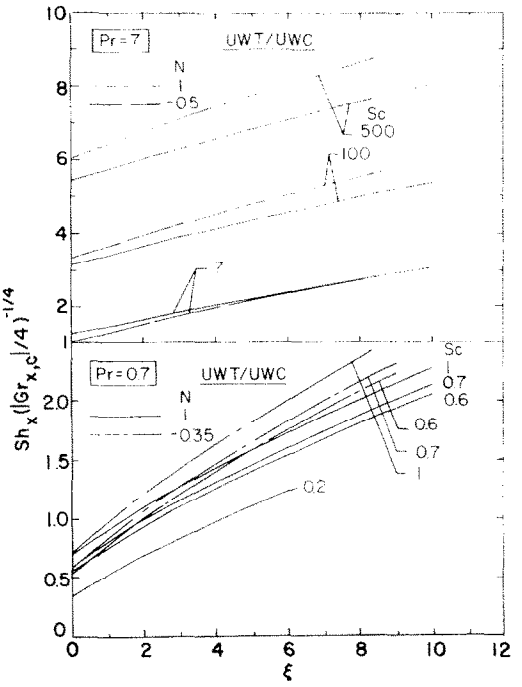

FIG. 3. Local Sherwood number results for uniform wall temperature/concentration, $Pr = 0.7$ and 7.

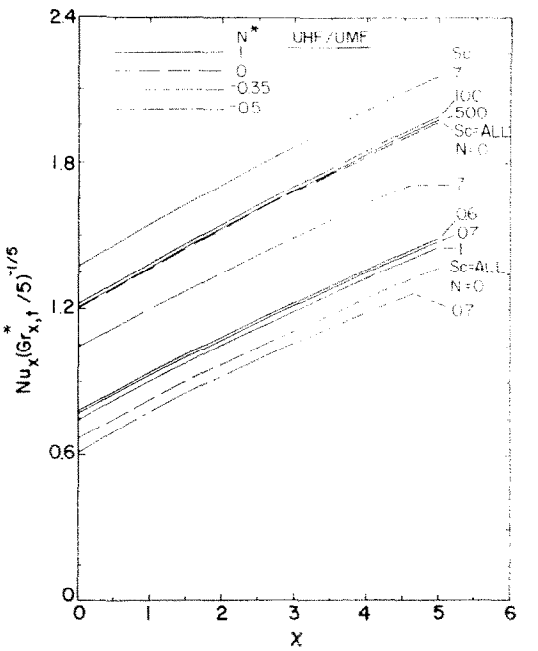

FIG. 5. Local Nusselt number results for uniform surface heat/mass flux, $Pr = 0.7$ and 7.

The wall shear stress $\tau_w(x^2/4\mu\nu)/(Gr_{x,t}/4)^{3/4}$ for the UWT/UWC case (Fig. 1) is seen to increase with increasing value of ξ, i.e. with increasing curvature of the cylinder. On the other hand, for the UHF/UMF case (Fig. 4), the quantity $\tau_w(x^2/5\mu\nu)/(Gr_{x,t}^*/5)^{3/5}$ decreases with an increase in χ. However, the decrease of this quantity does not mean that the wall shear stress τ_w decreases with increasing value of χ. Indeed, it actually *increases*, as will now be demonstrated. From equation (34) the wall shear stress τ_w for the UHF/UMF case is seen to be proportional to $x^{2/5}F''(\chi,0)$. In addition, from the χ expression in equation (22), one sees that $\chi \sim x^{1/5}$ or $x \sim \chi^5$. Thus, in terms of χ, one obtains $\tau_w \sim \chi^2 F''(\chi,0)$, and the wall shear stress ratio at two different χ values for the UHF/UMF case can be expressed as

$$(\tau_{w2}/\tau_{w1})_{UHF} = (\chi_2/\chi_1)^2[F''(\chi_2,0)/F''(\chi_1,0)]. \tag{48}$$

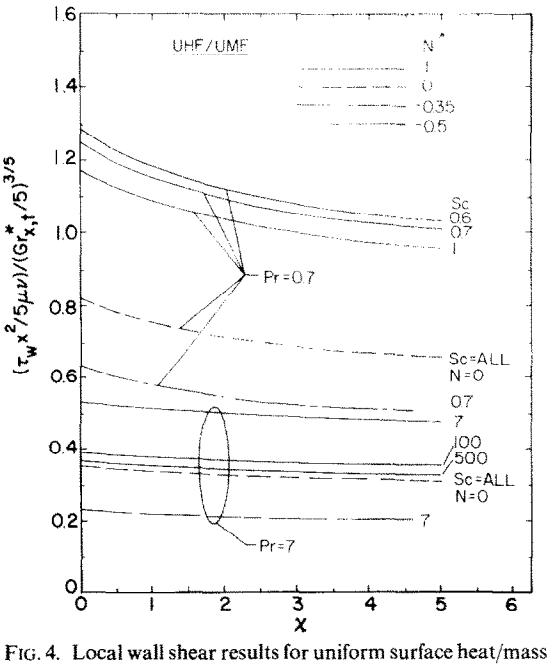

FIG. 4. Local wall shear results for uniform surface heat/mass flux, $Pr = 0.7$ and 7.

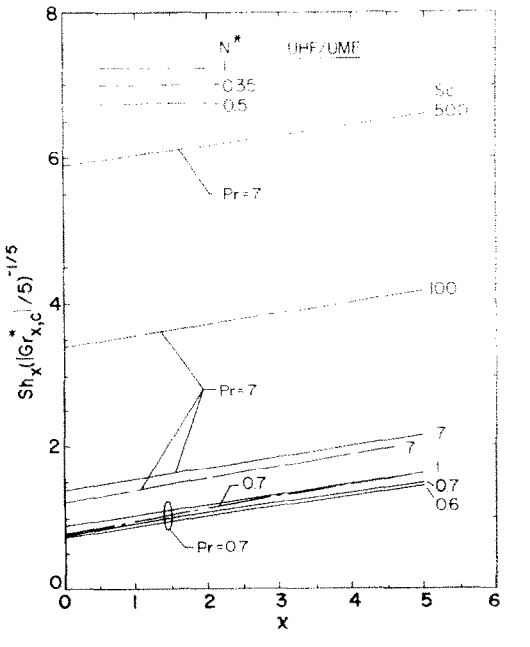

FIG. 6. Local Sherwood number results for uniform surface heat/mass flux, $Pr = 0.7$ and 7.

As an example, for $Pr = 0.7$, $Sc = 0.6$, and $N^* = 1$, the numerical results provide $F''(\chi_1, 0) = 1.1829$ for $\chi_1 = 1$ and $F''(\chi_2, 0) = 1.1211$ for $\chi_2 = 2$. This gives $(\tau_{w2}/\tau_{w1})_{UHF} = 3.791$. Thus, the actual wall shear stress *increases* with an increase in the χ value. From the analogy between heat and momentum transfer, an increase in the Nusselt number is a consequence of an increase in the wall shear stress, and vice versa. Figure 5 indicates that the local Nusselt number Nu_x increases with an increase in χ. Thus, τ_w should also increase with χ, as has just been demonstrated. Similarly, from the definition of ξ in equation (6) and τ_w in equation (19) one can derive for the UWT/UWC case

$$(\tau_{w2}/\tau_{w1})_{UWT} = (\xi_2/\xi_1)[f''(\xi_2, 0)/f''(\xi_1, 0)]. \tag{49}$$

For $Pr = 0.7$, $Sc = 0.6$, and $N = 1$, for example, one has $f''(\xi_1, 0) = 1.225$ when $\xi_1 = 0.931$ (corresponding to $\chi_1 = 1$) and $f''(\xi_2, 0) = 1.296$ when $\xi_2 = 1.932$ (corresponding to $\chi_2 = 2$). This gives $(\tau_{w2}/\tau_{w1})_{UWT} = 2.195$. Again, the actual wall shear stress for the UWT/UWC case is seen to increase with increasing ξ. A comparison between these two wall shear stress ratios suggests that, contrary to the conclusions one might have drawn from examining Figs. 1 and 4, the combined buoyancy force has a larger effect on the wall shear stress for the UHF/UMF case than for the UWT/UWC case. This agrees with the trend of Nusselt number ratio between the UHF and UWT cases, as will be explained later when Fig. 10 is presented.

An inspection of Figs. 1 and 4 also reveals that the values of the wall shear stress are larger for fluids with $Pr = 0.7$ (such as air) than for fluids with $Pr = 7$ (such as water). This is because of the lower Prandtl number of air which exhibits a greater velocity gradient and hence the shear stress at the wall. In contrast to the wall shear stress plots, the local Nusselt numbers for both UWT/UWC and UHF/UMF cases (Figs. 2 and 5) are seen to increase with increasing curvature of the cylinder. Furthermore, the local Nusselt numbers for $Pr = 7$ are larger than those for $Pr = 0.7$. This is to be expected, because a larger Prandtl number results in a thinner thermal boundary layer, with a corresponding larger temperature gradient at the wall and hence a larger surface heat transfer rate.

It is seen from Figs. 1, 2, 4, and 5 that as compared to the case of $N = 0$ or $N^* = 0$ (i.e. the case in which there is no mass diffusion and the buoyancy force arises solely from the temperature difference), both the wall shear stress and the local Nusselt number increase when the buoyancy force from mass diffusion acts in the same direction as the thermal buoyancy force to assist the flow (i.e. when $N > 0$ or $N^* > 0$) and decrease when the buoyancy force from mass diffusion acts in the opposite direction of the thermal buoyancy force to oppose the flow (i.e. when $N < 0$ or $N^* < 0$). Indeed, the combined buoyancy effects of thermal and mass diffusion are represented by the terms $\theta + N\lambda$ in equation (10) and $\phi + N^*\omega$ in equation (26), respectively, for the UWT/UWC and UHF/UMF cases. When the combinations of Pr, Sc, and N or N^* are such that $\theta + N\lambda > \theta$ or $\phi + N^*\omega > \phi$, the net buoyancy force contributes to an increase in both the wall shear stress and the local Nusselt number beyond their respective values for $N = 0$ or $N^* = 0$. On the other hand, if $\theta + N\lambda < \theta$ or $\phi + N^*\omega < \phi$, the net buoyancy force will contribute to a decrease in these two quantities below those for $N = 0$ or $N^* = 0$.

Inspection of Figs. 1, 2, 4, and 5 further indicates that a common trend exists among the wall shear and Nusselt number results. That is, larger departures of these quantities from $N = 0$ (or $N^* = 0$) are seen to be associated with smaller values of Schmidt numbers for both $N > 0$ (or $N^* > 0$) and $N < 0$ (or $N^* < 0$). This trend agrees with the physical reasoning in that a diffusing species with a smaller Schmidt number possesses a larger binary diffusion coefficient which will in return exert a larger effect on the flow and thermal fields.

The Sherwood number results (Figs. 3 and 6) show, as in the local Nusselt number plots, that the local Sherwood number increases with an increase in the curvature parameter ξ or χ. However, in contrast to the trend in the local Nusselt number results, larger

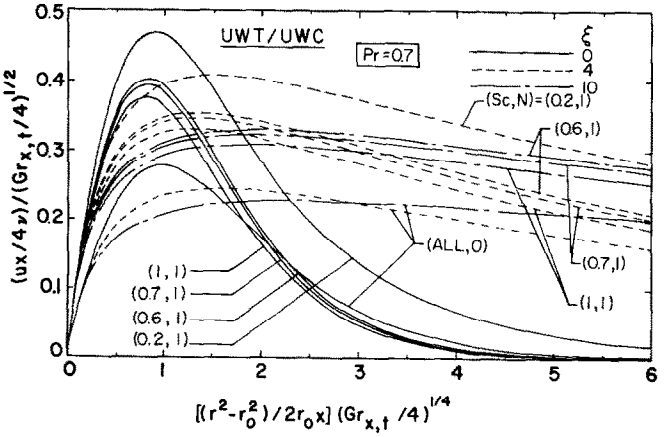

FIG. 7. Representative velocity profiles for uniform wall temperature/concentration, $Pr = 0.7$.

values of Schmidt number are seen to provide larger Sherwood numbers. This can be explained from the fact that a larger Schmidt number corresponds to a smaller binary diffusion coefficient for a given fluid and to a thinner concentration boundary layer relative to the flow boundary layer. This results in a larger concentration gradient at the wall (see Fig. 9) and hence a larger mass transfer rate or a larger Sherwood number. When N or N^* is very small (i.e. when the species diffusion is very small), heat transfer is not strongly affected by species diffusion (see Figs. 2 and 5), but the mass-transfer parameter or the Sherwood number becomes very large and exceeds that for a larger N or N^* value (see Fig. 3 and 6). This is because under this condition the flow is induced almost entirely by the thermal buoyancy force and the species diffusion mechanism becomes very effective at very low concentration levels. This accounts for the fact that for a given concentration Grashof number $Gr_{x,c}$ or $Gr^*_{x,c}$, the Sherwood number curves for smaller N or N^* values lie above those for larger N or N^* values. Since for a fixed concentration Grashof number $Gr_{x,c}$, a small N value implies a large thermal Grashof number $Gr_{x,t}$, it can be said that large Sherwood numbers occur when the thermal Grashof numbers are large compared to the concentration Grashof numbers.

It is to be noted here that there are no curves for $N = 0$ or $N^* = 0$ in Figs. 3 and 6. This is because the Sherwood number is undefined when $N = 0$ or $N^* = 0$, as this condition implies that there exists no concentration difference in the fluid or that the concentration level is negligibly small compared to the temperature difference in the fluid. In addition, the absolute quantities $|Gr_{x,c}/N|$ and $|Gr^*_{x,c}/N^*|$ are needed to ensure that the Sherwood numbers will be positive, for $Gr_{x,c}$, N, $Gr^*_{x,c}$, and N^* assume positive as well as negative values.

It is of practical interest to compare the present analytical results with experimental results. To the best knowledge of the authors, the only available experimental data for vertical cylinders are those of Bottemanne [6] for simultaneous heat transfer and evaporation of water vapor into still air (with $Pr = 0.71$ and $Sc = 0.63$) under the UWT/UWC condition. Bottemanne's experiments were conducted using a cylinder of "large diameter". Unfortunately, he did not mention the diameter of the cylinder. His experimental results are, in the notation of the present paper,

$$\theta'(\xi,0) = -0.52(1+N)^{1/4},$$
$$\lambda'(\xi,0) = -0.49(1+N)^{1/4}. \quad (50)$$

This gives, for example, $\theta'(\xi,0) = -0.6184$ and $\lambda'(\xi,0) = -0.5827$ for $N = 1$, and $\theta'(\xi,0) = -0.4669$ and $\lambda'(\xi,0) = -0.4400$ for $N = -0.35$. The present analysis for $Pr = 0.7$ and $Sc = 0.6$ under UWT/UWC condition provides (1) $\theta'(0,0) = -0.6007$, $\lambda'(0,0) = -0.5533$ for $N = 1$ and $\theta'(0,0) = -0.4426$, $\lambda'(0,0) = -0.4085$ for $N = -0.35$ when $\xi = 0$ (i.e. for a vertical plate) and (2) $\theta'(0.5,0) = -0.7267$, $\lambda'(0.5,0) = -0.6799$ for $N = 1$ and $\theta'(0.5,0) = -0.5368$, $\lambda'(0.5,0) = -0.5013$ for $N = -0.35$ when $\xi = 0.5$ (i.e. for a cylinder of relatively large diameter). From these comparisons, it is evident that the experimental data of Bottemanne for a large-diameter cylinder lie between the analytical results for $\xi = 0$ and $\xi = 0.5$ for both $N = 1$ and $N = -0.35$. Thus, it may be concluded that the agreement between the analysis and the experiment is fairly good.

Representative velocity, temperature, and mass fraction or concentration profiles for the UWT/UWC case with $Pr = 0.7$ are illustrated, respectively, in Figs. 7–9 for certain values of ξ, N, and Sc. The curves for $N = 0$ in Figs. 7 and 8 correspond to the situation in which there is no buoyancy force effect from mass diffusion. There are significant increases in the flow, thermal, and concentration boundary layer thicknesses as the value of ξ increases. However, a larger η_δ value associated with a larger ξ value does not accurately represent a larger boundary-layer thickness, as will now be explained. If $y = r - r_0$ is designated as the radial distance measured outward from the surface of the

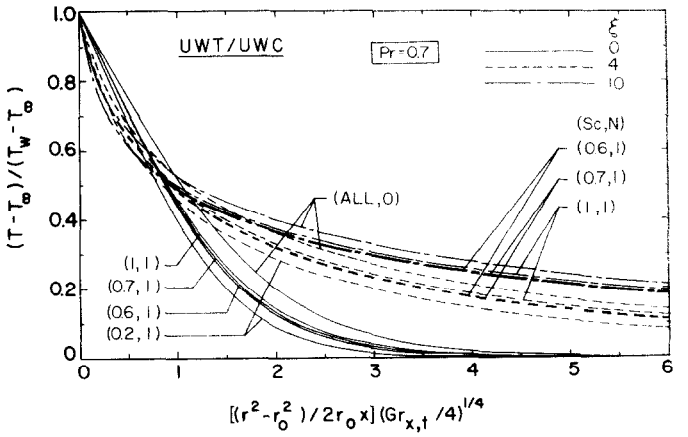

FIG. 8. Representative temperature profiles for uniform wall temperature/concentration, $Pr = 0.7$.

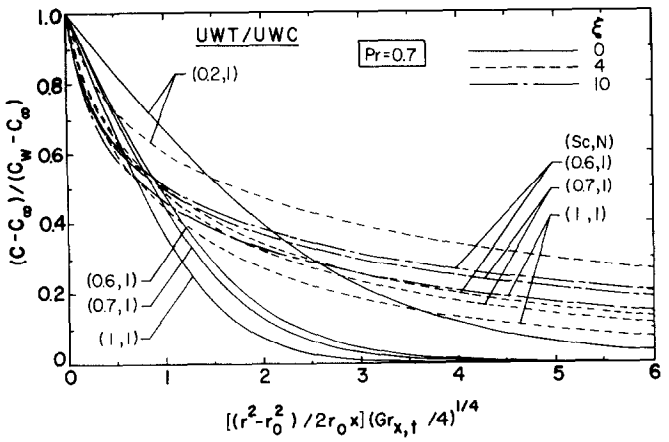

FIG. 9. Representative concentration profiles for uniform wall temperature/concentration, $Pr = 0.7$.

cylinder, the η coordinate in equation (6) can be written as

$$\eta = (y/x)(Gr_{x,t}/4)^{1/4}[(1 + r/r_0)/2]. \quad (51)$$

In addition, from the ξ and η definitions, one has

$$r/r_0 = (1 + \xi\eta)^{1/2} \quad (52)$$

Thus, for large values of ξ, r/r_0 may be substantially larger than one and the factor $(1 + r/r_0)/2$ that appears in equation (51) acts to increase the range of η for $\xi > 0$. However, this increased range of η does not mean that the range of $(y/x)\ (Gr_{x,t}/4)^{1/2}$, which is a more accurate measure of the boundary-layer thickness, has increased. Indeed, the range of this quantity could even decrease with increasing ξ, but the η value still increases because of the large increase in the factor $(1 + r/r_0)/2$.

For the velocity profiles (Fig. 7) the velocity gradient at the wall shows an increase with increasing values of N and ξ, but with decreasing value of Sc. This trend agrees with the friction factor results shown in Fig. 1. Indeed, if the combined buoyancy force effect is larger than the effect due to thermal buoyancy force alone, that is, if $\theta + N\lambda > \theta$, the velocity gradient at the wall will increase. On the other hand, it will decrease when the combined effect is less than the effect from thermal buoyancy force, i.e. when $\theta + N\lambda < \theta$. The temperature profiles (Fig. 8) show also that the wall temperature gradient increases as the values of ξ and N increase and the value of Sc decreases. This behavior is consistent with the Nusselt number results shown in Fig. 2. As with the velocity gradient, the temperature gradient at the wall increases above that for $N = 0$ when $\theta + N\lambda > \theta$ and decreases below it when $\theta + N\lambda < \theta$.

The concentration or mass fraction profiles (Fig. 9) exhibit trends that are somewhat different from those of the velocity and temperature profiles. While the concentration gradient at the wall increases as ξ increases, a larger increase is associated with a larger Schmidt number. The effect caused by the Schmidt number on the concentration field is similar to the Prandtl number effect on the thermal field that was explained when the Nusselt number results were presented.

Finally, the Nusselt number ratios $(Nu_x)_{UHF}/(Nu_x)_{UWT}$ between the UHF and UWT cases are plotted against the equivalent curvature parameter ξ_e in Fig. 10. Curves are shown only for the cases of $Sc = Pr$ and $N^* = N$. It can be seen from the figure that the Nusselt numbers for the UHF case are higher than those for the UWT case. As ξ_e increases, the Nusselt number ratio decreases and becomes a constant at large values of ξ_e. For $Pr = 0.7$, the Nusselt number ratio starts with a value larger than that for $Pr = 7$ at $\xi_e = 0$, but it becomes smaller at larger ξ_e values. In addition, it is seen that the Nusselt Number ratio decreases as the value of $N^* = N$ decreases. As was explained in the Analysis Section, the Sherwood number ratio $(Sh_x)_{UMF}/(Sh_x)_{UWC}$ is exactly identical to

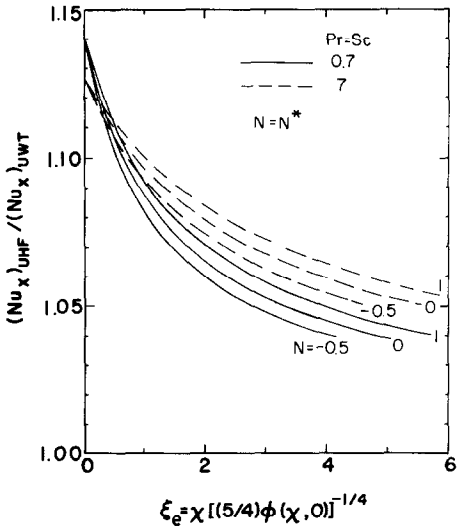

FIG. 10. Nusselt number ratio and Sherwood number ratio for $Sc = Pr$ and $N^* = N$.

the $(Nu_x)_{UHF}/(Nu_x)_{UWT}$ ratio when $Sc = Pr$ and $N^* = N$, with $\xi = \xi_e$. Thus, the curves in Fig. 10 also apply to the Sherwood number ratios.

CONCLUSION

The present study on natural convection on a vertical cylinder under the combined buoyancy force effects of thermal and species diffusion indicates that the local Nusselt number and the local Sherwood number increase with increasing curvature of the cylinder. The local Nusselt number increases and decreases as the buoyancy force from species diffusion assists and opposes, respectively, the thermal buoyancy force. The mass transfer is found to become more effective as the thermal buoyancy force increases. While the local surface heat transfer is enhanced as the Schmidt number is decreased, the surface mass transfer increases with increasing Schmidt number. In addition, both the local Nusselt number and the local Sherwood number have larger values for $Pr = 7$ than for $Pr = 0.7$. The combined buoyancy force from thermal and mass diffusion has been found to provide larger Nusselt and Sherwood numbers under uniform surface heat/mass flux than under uniform wall temperature/concentration.

Acknowledgement The present study was funded by a grant (NSF ENG 75-15033 A01) from the National Science Foundation.

REFERENCES

1. B. Gebhart and L. Pera, The nature of vertical natural convection flows resulting from the combined buoyancy effects of thermal and mass diffusion, *Int. J. Heat Mass Transfer* **14**, 2025–2050 (1971).
2. L. Pera and B. Gebhart, Natural convection flows adjacent to horizontal surfaces resulting from the combined buoyancy effects of thermal and mass diffusion, *Int. J. Heat. Mass Transfer* **15**, 269–278 (1972).
3. T. S. Chen and C. F. Yuh, Combined heat and mass transfer in natural convection on inclined surfaces, *Numer. Heat Transfer* **2**, 233–250 (1979).
4. W. J. Minkowycz and E. M. Sparrow, Local nonsimilar solutions for natural convection on a vertical cylinder, *J. Heat Transfer* **96**, 178–183 (1974).
5. T. Cebeci and P. Bradshaw, *Momentum Transfer in Boundary Layers*, Chapter 7, Hemisphere, Washington, D.C. (1977).
6. F. A. Bottemanne, Experimental results of pure and simultaneous heat and mass transfer by free convection about a vertical cylinder for $Pr = 0.71$ and $Sc = 0.63$, *Appl. Scient. Res.* **25**, 372–382 (1972).

TRANSFERT SIMULTANE DE CHALEUR ET DE MASSE EN CONVECTION NATURELLE LE LONG D'UN CYLINDRE VERTICAL

Résumé — Dans un étude analytique, on considère le transfert de chaleur et de masse pour un écoulement de convection naturelle le long d'un cylindre vertical, sous l'effet combiné de la diffusion thermique et des espèces. L'analyse est réduite au cas où les effets de la thermodiffusion aussi bien que des vitesses interfaciales provenant de la diffusion des espèces sont négligeables. La surface du cylindre est soit à température/concentration uniforme soit à flux de chaleur/masse uniforme. Parmi les paramètres principaux, on note la courbure du cylindre, les nombres de Prandtl et de Schmidt, les nombres de Grashof thermique et massique et l'effet relatif des forces dues à la diffusion de chaleur et de masse. Des résultats numériques sont présentés pour la diffusion d'espèces dans l'air et dans l'eau. Pour les deux conditions de chauffage et de diffusion, la tension pariétale locale, les nombres de Nusselt et de Sherwood locaux croissent avec la courbure du cylindre. De plus, les deux premières grandeurs augmentent ou diminuent selon que la force d'Archimède dûe à la diffusion massique assiste ou s'oppose à celle dûe à la diffusion thermique. Ce paramètre de transfert massique ou le nombre de Sherwood local est augmenté lorsque la force d'origine thermique croît. Enfin, les forces combinées d'origine thermique et massique conduisent à des nombres de Nusselt et de Sherwood plus grands pour les conditions surfaciques de flux thermique/massique uniforme que pour les conditions de température/concentration uniforme.

GLEICHZEITIGER WÄRME- UND STOFFÜBERGANG BEI FREIER KONVEKTION LÄNGS EINES VERTIKALEN ZYLINDERS

Zusammenfassung—Eine analytische Untersuchung wird durchgeführt, um das Wärme- und Stoffübergangsverhalten bei freier Konvektions-strömung entlang eines vertikalen Zylinders unter den kombinierten Einflüssen der Auftriebsdkräfte von Wärmeleitung und Diffusion zu analysieren. Die Analyse ist auf Vorgänge beschränkt, bei denen sowohl die Diffusionsthermo- und Thermodiffusions-Effekte, als auch die Grenzflächengeschwindigkeiten infolge der Stoffdiffusion vernachlässigbar sind. Die Oberfläche des Zylinders wird entweder auf gleichmäßiger Temperatur bzw. Konzentration gehalten, oder einer gleichmäßigen Wärme- bzw. Massenstromdichte unterworfen. Die Hauptparameter des Problems sind Krümmung des Zylinders, Prandtl- und Schmidt-Zahlen, thermische und konzentrationsbezogene Grashof-Zahl und das Verhältnis zwischen den thermisch und konzentrationsbedingten Auftriebskrafteffekten. Zahlenmäßige Ergebnisse werden erhalten und für den interessierenden Bereich der Stoffdiffusionen in Wasser und Luft angegeben. Sowohl bei Heizungs-wie auch bei Diffusionsbedingungen nehmen die örtliche Wandschubspannung, die örtliche Nusselt-Zahl und die örtliche Sherwood-Zahl mit zunehmender Krümmung des Zylinders zu. Außerdem wurde gefunden, daß die ersten zwei Größen zu- oder abnehmen, je nachdem die Auftriebskraft infolge der Stoffdiffusion die thermische Auftriebskraft unterstützt oder ihr entgegengerichtet ist. Der Stoffübergangsparameter oder die örtliche Sherwood-Zahl wird mit zunehmender thermischer Auftriebskraft größer. Schließlich liefert die kombinierte Auftriebskraft durch Wärmeleitung und Stoffdiffusion für gleichmäßige Wärme- bzw. Stoffstromdichten an der Oberfläche größere Nusselt- und Sherwood-Zahlen als für gleichförmige Wandtemperaturen bzw. Wandkonzentrationen.

СОВМЕСТНЫЙ ТЕПЛО- И МАССОПЕРЕНОС ПРИ ЕСТЕСТВЕННОЙ КОНВЕКЦИИ ВДОЛЬ ВЕРТИКАЛЬНОГО ЦИЛИНДРА

Аннотация — Проведен анализ тепло- и массообменных характеристик естественно-конвективного течения вдоль вертикального цилиндра при совместном действии подъёмных сил, обусловленных диффузией тепла и вещества. Анализ ограничен процессами, в которых диффузионный термоэффект и термодиффузионный эффект, а также величина скорости на поверхности цилиндра, обусловленная диффузией вещества, пренебрежимо малы. Поверхность цилиндра или находится при постоянной температуре–концентрации или подвержена действию однородного теплового–массового потока. Основные параметры задачи включали кривизну цилиндра, числа Прандтля и Шмидта, тепловое и концентрационное числа Грасгофа, а также отношение подъёмных сил, обусловленных диффузией вещества и тепла. Получены численные результаты для диффузии в воздухе и воде. Как для тепловых, так и для диффузионных граничных условий, значения локального напряжения сдвига на стенке, локального числа Нуссельта и локального числа Шервуда увеличиваются с ростом кривизны цилиндра. Кроме того найдено, что первые две величины возрастают или уменьшаются в зависимости от того, направлена ли подъёмная сила, обусловленная диффузией вещества, в сторону действия тепловой подъёмной силы или в противоположном ей направлении. Параметр массообмена или локальное число Шервуда возрастает по мере увеличения значения тепловой подъёмной силы. Наконец, при одновременном действии диффузии тепла и вещества значения чисел Нуссельта и Шервуда для однородного потока тепла–массы на поверхности выше, чем для постоянной температуры–концентрации на стенке.